View Article Online / Journal Homepage / Table of Contents for this issue

Theoretical studies on structures and spectroscopic properties of a series of novel mixed-ligand Ir(III) complexes [Ir(Mebib)(ppy)X]

Tao Liu,[a] Hong-Xing Zhang,*[a] Xin Shu[a] and Bao-Hui Xia[a,b]

Received 11th January 2007, Accepted 5th March 2007
First published as an Advance Article on the web 23rd March 2007
DOI: 10.1039/b700407a

Published on 23 March 2007. Downloaded by Michigan State University on 21/01/2016 12:05:07.

The series of novel mixed-ligand iridium(III) complexes Ir(Mebib)(ppy)X (Mebib = bis(N-methylbenzimidazolyl)benzene and ppy = phenylpyridine; X = Cl, **1**; X = –C≡CH, **2**; X = CN, **3**) have been investigated theoretically to explore their electronic structures and spectroscopic properties. The ground and excited state geometries have been fully optimized at the B3LYP/LANL2DZ and CIS/LANL2DZ levels, respectively. The optimized geometry structural parameters agree well with the corresponding experimental results. The HOMO of **1** and **3** are mainly localized on the Ir atom, Mebib, and ppy ligand, but that of **2** has significant X ligand composition. Absorptions and phosphorescences in CH_2Cl_2 media have been calculated using the TD-DFT level of theory with the PCM model based on the optimized ground and excited state geometries, respectively. The lowest lying absorptions of **1** and **3** at 444 and 416 nm are attributed to a $\{[d_{yz}(Ir) + \pi(Mebib) + \pi(ppy)] \rightarrow [\pi^*(Mebib)]\}$ transition with metal-to-ligand, ligand-to-ligand, and intra-ligand charge transfer (MLCT/LLCT/ILCT) character, whereas that of **2** at 458 nm is related to a $\{[d_{yz}(Ir) + \pi(Mebib) + \pi(ppy) + \pi(C{\equiv}CH)] \rightarrow [\pi^*(Mebib)]\}$ transition with MLCT/LLCT/ILCT and X ligand-to-ligand charge transfer (XLCT) transition character. The phosphorescence of **1** and **3** at 565 and 543 nm originates from the $^3\{[d_{yz}(Ir) + \pi(Mebib) + \pi(ppy)]\ [\pi^*(Mebib)]\}$ excited state, while that of **2** at 576 nm originates from the $^3\{[d_{yz}(Ir) + \pi(Mebib) + \pi(ppy) + \pi(C{\equiv}CH)]\ [\pi^*(Mebib)]\}$ excited state. The calculation results show that the absorption and emission transition character can be changed by altering the π electron-withdrawing ability of the X ligand and the phosphorescent color can be tuned by adjusting the X ligand.

Introduction

Organometallic complexes have attracted much attention in recent years, especially Os(II), Ru(III), and Ir(III) complexes with d^6 electronic configuration. The spectral properties of these transition metal complexes have been investigated extensively in experimental and theoretical studies because of their successful applications in OLEDs,[1] biological labeling reagents,[2] sensors,[3] and photocatalysts for CO_2 reduction.[4] Due to the strong spin–orbital coupling effects of the heavy transition metals, the triplet metal-to-ligand charge transfer (^{3}MLCT) excited state can emit effectively by borrowing the intensity of the singlet MLCT excited state, thus, in theory, OLEDs based on phosphorescence have higher internal quantum efficiency (more than 75%) compared with those based on fluorescence (25%).[5]

After it was reported that OLEDs prepared with $Ir(ppy)_3$ (ppy^- = 2-phenylpyridine) have efficiencies of more than 80%, Ir(III) complexes have attracted much more attention.[6–11] Numerous bis- and tris-cyclometalated iridium complexes such as $Ir(C\hat{N})_3$ ($C\hat{N}$ = 1-phenylpytazolato (ppz) and 2-(4,6-difluorophenyl)pyridimato (46dfppy) *etc.*), $Ir(C\hat{N})_2L$ ($C\hat{N}$ = benzoquinoline (bzq), 2-(4-tolyl)pyridine (tpy), 2-(2′-thienyl)pyridine (thp); L = acetoylacetonate (acac), dibenzoylmethanate (dbm)), and $[IrLL']^{n+}$ (L, L′ = terpyridine derivative; n = 2 or 3) have been synthesized and their spectral properties have been investigated by Thompson *et al.*,[6,12] Hay *et al.*,[8] and Collin *et al.*[13] both experimentally and theoretically. Moreover, $[Ir(ppy)_2(L)_2]^-$ (L = CN, NCS, and NCO) has been reported to exhibit unprecedented high quantum yields by Nazeeruddin and co-workers.[14] They came to the conclusion that the phosphorescence predominantly originates from three triplet excited states including a triplet intra-ligand charge transfer (^{3}ILCT), triplet ligand-to-ligand charge transfer (^{3}LLCT), and ^{3}MLCT. Moreover, the phosphorescent color can be adjusted from green to red by tuning the $C\hat{N}$ and L ligands.

Although these Ir complexes are suitable for emitter applications, it is difficult for other groups to access the Ir atom in such structures, so only the limited number of luminescent Ir(III) complexes discussed above have been reported. Recently, a series of novel mixed-ligand Ir(III) complexes $[Ir(L)(N\hat{C})X]^{n+}$ (L = $N\hat{C}\hat{N}$ or $N\hat{N}\hat{N}$; X = Cl, Br, I, CN, $–CH_3CN$, or –CCPh; n = 0 or 1) have been synthesized, and the X-ray crystal structures, absorption and emission spectra have been investigated by Haga and co-workers.[15] This kind of mixed-ligand Ir(III) complex has shown a higher luminescence quantum yield (~0.8) and it is easy to adjust the ligand to obtain suitable luminescent materials. Furthermore, they performed part of the theoretical studies on frontier molecular orbitals based on the X-ray geometry structure parameters without geometry optimization using the time-dependent density functional theory[16] (TDDFT) method.

From the above background, we carried out the present work, aimed at providing an in-depth theoretical understanding of the electronic structures and spectroscopic properties of the mixed-ligand Ir(III) complexes as well as the relationship

[a]*State Key Laboratory of Theoretical and Computational Chemistry, Institute of Theoretical Chemistry, Jilin University, Changchun, 130023, P.R. China. E-mail: Zhanghx@mail.jlu.edu.cn*
[b]*College of Chemistry, Jilin University, Changchun, 130023, P.R. China*

 This journal is © The Royal Society of Chemistry 2007

View Article Online

Published on 23 March 2007. Downloaded by Michigan State University on 21/01/2016 12:05:07.

between the spectra and the X ligand. Herein, we performed theoretical calculations on Ir(Mebib)(ppy)X[15] (Mebib = bis(N-methylbenzimidazolyl)benzene and ppy = phenylpyridine; X = Cl **1**; X = –C≡CH, **2**; X = CN, **3**) using *ab initio* and density functional theory[17] (DFT) methods. Importantly, the effects of the peripheral X ligand on the phosphorescence have been revealed so that the phosphorescent color can be tuned by adjusting X ligands.

Computational methods

The calculated complexes display C_s symmetry both in the ground and the excited states. As shown in Fig. 1, the *y* axis stays on the Ir atom and along the Ir–X bond, while the *x* axis is oriented through the Ir and C(1) atoms, and the Mebib ligand lies on the *xz* plane. The Mebib and the ppy ligands are almost perpendicular to each other. The geometry structures in the ground and excited states were fully optimized by the DFT method with Becke's three parameter functional and the Lee–Yang–Parr functional[18] (B3LYP) and the configuration interaction with single-excitations[19] (CIS) approach, respectively. On the basis of the optimized geometry structures in the ground and excited states, the absorption and emission in dichloromethane (CH_2Cl_2) were calculated by the TDDFT method associated with the polarized continuum model[20] (PCM). This kind of theoretical approach has been proven to be reliable for transition metal complex systems.[21]

In the calculations, the quasi-relativistic pseudo-potentials of Ir atoms proposed by Hay and Wadt[22] with 17 valence electrons were employed, and a "double–ξ" quality basis set LANL2DZ associated with the pseudo-potential was adopted. A relative effective core potential (ECP) on Ir replaced the inner core electrons leaving the outer core [$(5s^2)(5p^6)$] electrons and the ($5d^6$) valence electrons for Ir(III). The basis sets were described as Ir [8s6p3d]/[3s3p2d], C and N [10s5p]/[3s2p], Cl [3s3p]/[2s2p], and H [4s]/[2s]. Thus, 422 basis functions and 282 electrons for **1**, 434 basis functions and 288 electrons for **2**, and 432 basis functions and 288 electrons for **3** have been included in the calculations. All of the calculations were accomplished by using the Gaussian 03 software package[23] on an Origin/3900 server.

Results and discussion

Geometries and frontier molecular orbital compositions in the ground state

The calculated results reveal that all of the complexes have a $X\,^1A'$ ground state. The main optimized geometry structural parameters in the ground state together with the X-ray crystal diffraction data of [Ir(Mebib)(mppy)Cl][15] are given in Table 1 and the optimized geometries are shown in Fig. 1.

Fig. 1 shows that there may be two types of geometry structures for this kind of Ir complex, isomer A (N(3) atom is located *trans* to the Ir–C(1) bond) and isomer B (C(2) atom is located *trans* to the Ir–C(1) bond). Take **1** for example, our calculated results show that isomer A is more stable than isomer B because the energy of isomer A is lower than that of isomer B by about 0.71 eV, which results in isomer B turning into isomer A by the interaction of the molecule. In addition, the X-ray results also confirmed that this kind of Ir complex adopts structure A.[15]

The optimized structures show that the Mebib ligand is almost coplanar because the C(1)–C(3)–C(4)–N(2) dihedral angle is close to 0°, which is consistent with the X-ray results. The optimized bond lengths and bond angles of **1–3** in the ground state are in general agreement with the corresponding experimental values of [Ir(Mebib)(mppy)Cl].[15] The calculated bond lengths of Ir–C(1) (1.964 Å), Ir–N(3) (2.158 Å), Ir–C(2) (2.028 Å), and Ir–Cl (2.560 Å) are overestimated by about 0.01–0.08 Å except that the Ir–N(1) bond length is underestimated by about 0.003 Å in comparison with the measured values. The calculated bond

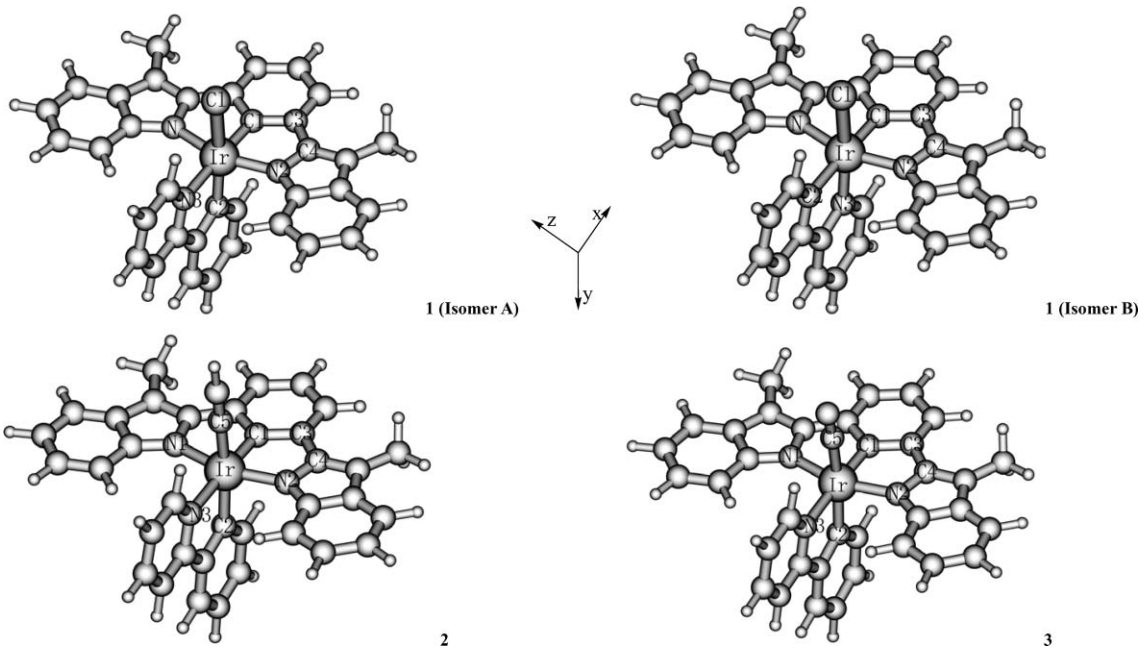

Fig. 1 The optimized geometries of **1** (isomer A and B)**2**, and **3** at the B3LYP/LANL2DZ level.

View Article Online

Published on 23 March 2007. Downloaded by Michigan State University on 21/01/2016 12:05:07.

Table 1 The main optimized geometry structural parameters of **1–3** in the ground and the lower-lying triplet excited state at the B3LYP and CIS level respectively, together with the experimental values of Ir(Mebib)(mppy)Cl

	1		**2**		**3**		Ir(Mebib)(mppy)Cl
Parameter	$^1A'$	$^3A'$	$^1A'$	$^3A'$	$^1A'$	$^3A'$	Exptl[a]
Bond length/Å							
Ir–N(1)	2.068	2.097	2.072	2.100	2.074	2.100	2.071
Ir–C(1)	1.964	1.989	1.959	1.987	1.965	1.990	1.922
Ir–N(3)	2.158	2.175	2.172	2.181	2.168	2.177	2.142
Ir–C(2)	2.028	2.049	2.081	2.099	2.072	2.087	2.001
Ir–Cl	2.560	2.575					2.487
Ir–C(5)			2.065	2.098	2.071	2.105	
Bond angle/°							
N(1)–Ir–N(2)	158.4	157.2	158.3	157.0	158.2	157.0	157.7
C(1)–Ir–N(2)	79.2	78.6	79.2	78.5	79.1	78.5	79.2
C(2)–Ir–Cl	171.5	172.5					172.1
C(2)–Ir–C(5)			170.7	173.0	170.7	172.9	
Dihedral angle/°							
C(1)–C(3)–C(4)–N(2)	0.8	0.8	0.7	0.6	0.7	0.6	

[a] From ref. 15.

angles deviate slightly (1.0°) from the experimental values. The discrepancy of the geometry structural data between the calculated and measured values is reasonable and acceptable because the environments of the complexes are different in the two cases: in the latter case, the molecule is in a tight crystal lattice, while in the former case, the molecule is free.

The frontier molecular orbital compositions and energies of **1**, **2**, and **3** are given in Tables 2, 3, and 4, respectively. Table 2 shows that the highest occupied molecule orbital (HOMO) of **1** is mainly composed of 49.4% d_{yz}(Ir), 27.0% π(Mebib), 18.9% π(ppy), and 4.7% π(Cl), while that of **3** has a similar composition (see Table 4). But with respect to the HOMO of **2**, the contribution from the –C≡CH ligand is increased to 12.0% (see Table 3). The calculated results show that with an increase in the π electron-withdrawing abilities in the order –C≡CH < Cl < CN, the contribution of the X ligand to the HOMO increases in the order **3** < **1** < **2**. Furthermore, with respect to the HOMO−1 of **1**, **2** and **3**, there is a similar relationship between composition and π electron-withdrawing ability of the X ligand. The energy levels of the HOMO change more significantly than those of the LUMO and are increasing in the order **3** < **1** < **2**, which is consistent with a decreasing trend in the π electron-withdrawing ability of X ligands CN > Cl > –C≡CH. The calculated results indicate that an X ligand with a stronger π electron-withdrawing ability can decrease the energy level of the HOMO more markedly than those of the LUMO resulting in broader HOMO–LUMO (H–L) gaps. The

Table 2 Molecular orbital compositions (%) in the ground state for Ir(Mebib)(ppy)Cl (**1**) at B3LYP level

		MO composition					
Orbital	Energy/eV	Ir	Mebib	ppy	Cl	Main bond nature	Ir orbital
92a′	0.0737	0.7	96.5	2.5	0.3	π*(Mebib)	
54a″	−1.5364	3.0	6.5	90.4	0.1	π*(ppy)	
53a″	−1.8381	1.6	97.0	1.4	0.0	π*(Mebib)	
HOMO LUMO gap							
52a″	−5.2178	49.4	27.0	18.9	4.7	d(Ir) + π*(Mebib) + π*(ppy)	d_{yz}
89a′	−5.4992	44.6	43.0	5.9	6.5	d(Ir) + π*(Mebib)	d_{xy}
88a′	−6.2989	9.6	69.3	5.3	15.8	π*(Mebib) + π*(Cl)	
86a′	−6.9275	4.8	52.6	17.4	25.2	π*(Mebib) + π*(ppy) + π*(Cl)	

Table 3 Molecular orbital compositions (%) in the ground state for Ir(Mebib)(ppy)CCH (**2**) at B3LYP level

		MO composition					
Orbital	Energy/eV	Ir	Mebib	ppy	C≡CH	Main bond nature	Ir orbitals
57a″	0.2193	0.4	92.1	7.5	0.0	π*(Mebib)	
55a″	−0.9853	1.5	3.8	94.6	0.1	π*(ppy)	
53a″	−1.7826	1.6	97.6	0.8	0.0	π*(Mebib)	
HOMO LUMO gap							
52a″	−5.0766	49.5	22.6	15.9	12.0	d(Ir) + π*(Mebib) + π*(ppy) + π*(C≡CH)	d_{yz}
92a′	−5.2595	42.4	33.2	9.1	15.3	d(Ir) + π*(Mebib) + π*(C≡CH)	d_{xy}
91a′	−6.1166	2.5	70.5	5.4	21.6	π*(Mebib) + π*(C≡CH)	
49a″	−6.2143	1.9	37.8	44.0	16.3	π*(Mebib) + π*(ppy) + π*(C≡CH)	

 This journal is © The Royal Society of Chemistry 2007

View Article Online

Published on 23 March 2007. Downloaded by Michigan State University on 21/01/2016 12:05:07.

Table 4 Molecular orbital compositions (%) in the ground state for Ir(Mebib)(ppy)CN (**3**) at B3LYP level

		MO composition					
Orbital	Energy/eV	Ir	Mebib	ppy	CN	Main bond nature	Ir orbital
95a′	0.0590	0.3	98.0	1.4	0.3	π*(Mebib)	
56a″	−0.1527	0.2	98.2	1.6	0.0	π*(Mebib)	
53a″	−1.8877	1.4	97.9	0.7	0.0	π*(Mebib)	
HOMO LUMO gap							
52a″	−5.4293	46.1	30.4	20.2	3.3	d(Ir) + π*(Mebib) + π*(ppy)	d_{yz}
92a′	−5.6328	36.5	51.6	7.3	4.6	d(Ir) + π*(Mebib)	d_{xy}
91a′	−6.3675	5.6	73.5	14.6	6.3	π*(Mebib) + π*(CN)	

LUMOs of **1–3** localized on the Mebib ligand with more than 97.0% composition are hardly changed by the variation of the X ligands.

Absorptions in CH_2Cl_2 media

The calculated absorptions and their oscillator strengths, the main configurations, and their assignments as well as the experimental results[15] are given in Table 5. The fitted Gaussian type absorption curves are shown in Fig. 2. To intuitively understand the transition process, the energy levels of molecular orbital involved in transitions of **1–3** are displayed in Fig. 3.

Fig. 2 shows the lowest lying distinguishable absorption bands at 444 nm (2.79 eV), 458 nm (2.71 eV), and 416 nm (2.98 eV) for **1**, **2**, and **3**, respectively. Table 5 shows that excitation of MO 52a″ → MO 53a″ with the configuration coefficient of 0.672 is responsible for the absorption band of **1** at 444 nm. From the above discussion on the frontier molecular orbitals, this absorption transition can be described as a {[d_{yz}(Ir) + π(Mebib) + π(ppy)] → [π*(Mebib)]} transition with MLCT, intraligand charge transfer (ILCT), and LLCT transition character, while the lowest lying absorption band of complex **3** at 416 nm has a similar transition path to that for

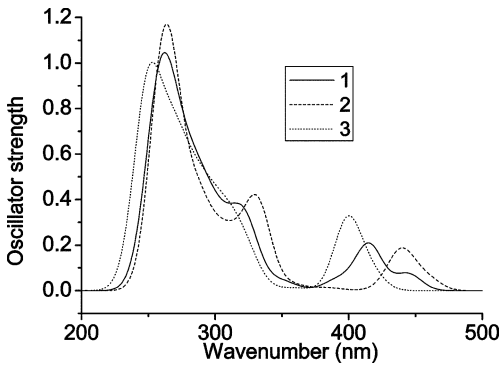

Fig. 2 The simulated absorption spectra of **1–3** in CH_2Cl_2 media with the data calculated at the TD-DFT/LANL2DZ level.

1 at 444 nm. But for **2**, the excitation of MO 52a″ → MO 53a″ (CI = 0.682) is responsible for the absorption at 458 nm, the above frontier molecular orbitals discussion shows that the MO 52a″ includes a 12.0% contribution from the –C≡CH ligand, so this absorption is assigned to {[d_{yz}(Ir) + π(Mebib) + π(ppy) + π(C≡CH)] → [π*(Mebib)]} transition with MLCT/ILCT/LLCT and X ligand-to-ligand charge transfer (XLCT) character.

Table 5 The absorptions of **1–3** calculated using the TDDFT method, together with the experimental values

	Transition	Config. (CI coeff)	*E*/nm (eV)	Oscillator	Assignment	λ_{exptl}/nm (eV)[a]
Singlet → Singlet						
1	$X^1A' \rightarrow A^1A'$	52a″ → 53a″ (0.672)	444 (2.79)	0.075	MLCT/LLCT/XLCT	472 (2.63)
	$X^1A' \rightarrow B^1A''$	89a′ → 53a″ (0.662)	415 (2.99)	0.198	MLCT/XLCT/ILCT	425 (2.92)
	$X^1A' \rightarrow C^1A''$	88a′ → 53a″ (0.664)	321 (3.86)	0.216	ILCT/XLCT	360 (3.44), 299 (4.15)
	$X^1A' \rightarrow D^1A''$	52a″ → 92a′ (0.444) 86a′ → 54a″ (0.369)	260 (4.77)	0.230	MLCT/XLCT/ILCT LLCT/XLCT	244 (5.08)
2	$X^1A' \rightarrow A^1A''$	52a″ → 53a″ (0.682)	458 (2.71)	0.054	MLCT/XLCT/LLCT	
	$X^1A' \rightarrow B^1A''$	92a′ → 53a″ (0.685)	439 (2.82)	0.174	MLCT/XLCT	
	$X^1A' \rightarrow C^1A''$	91a′ → 53a″ (0.680)	332 (3.73)	0.301	XLCT/ILCT	
	$X^1A' \rightarrow D^1A'$	52a″ → 57a″ (0.540) 49a″ → 55a″ (0.303)	262 (4.74)	0.219	MLCT/XLCT/LLCT ILCT	
3	$X^1A' \rightarrow A^1A'$	52a″ → 53a″ (0.676)	416 (2.98)	0.078	MLCT/LLCT/XLCT	413 (3.00)
	$X^1A' \rightarrow B^1A''$	92a′ → 53a″ (0.679)	399 (3.11)	0.298	MLCT/XLCT/ILCT	392 (3.16)
	$X^1A' \rightarrow C^1A'$	91a′ → 53a″ (0.609)	316 (3.93)	0.083	MLCT/LLCT	353 (3.51)
	$X^1A' \rightarrow D^1A''$	52a″ → 95a′ (0.455) 92a′ → 56a″ (0.453)	252 (4.92)	0.227	MLCT/ILCT/LLCT MLCT/ILCT	242 (5.12)
Singlet → Triplet						
1	$X^1A' \rightarrow A^1A'$	52a″ → 53a″ (0.677)	526 (2.36)		MLCT/LLCT/XLCT	523 (2.37)
2	$X^1A' \rightarrow B^1A''$	52a″ → 53a″ (0.679)	532 (2.33)		MLCT/LLCT/XLCT	
3	$X^1A' \rightarrow C^1A''$	52a″ → 53a″ (0.659)	504 (2.46)		MLCT/LLCT/XLCT	506 (2.45)

[a] From ref. 15.

View Article Online

Published on 23 March 2007. Downloaded by Michigan State University on 21/01/2016 12:05:07.

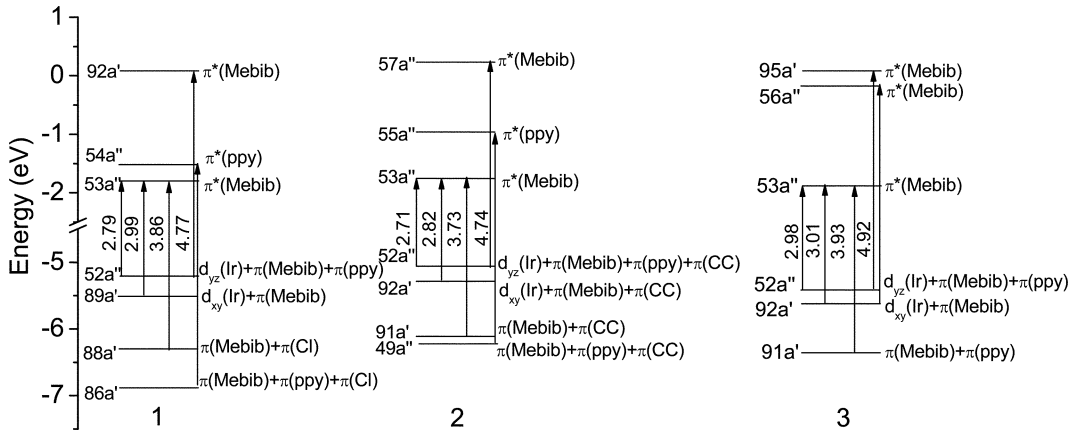

Fig. 3 Diagrams of the molecular orbitals related to the absorptions for **1–3**.

By comparing the absorptions of **1–3** at 444, 458, and 416 nm, we find that the lowest lying absorptions are red-shifted in the order **3**, **1**, **2**. Given the decreasing trend of the π electron-withdrawing ability of X ligands CN > Cl > –C≡CH, we can conclude that there will be a larger red shift if the π electron-withdrawing ability of X is weaker. In addition, the excitation energy levels of the absorption band lying directly above the lowest lying band show similar trends to those of the lowest lying absorptions. Table 5 shows that the absorption transition $X\,^1A'' \rightarrow B\,^1A''$ of **1**, **2**, and **3** are at 415 nm (2.99 eV), 439 nm (2.82 eV), and 399 nm (3.11 eV), respectively, and are mainly contributed by the excitation from HOMO−1 to LUMO. With respect to **1**, the excitation of MO 89a′ → MO 53a″ with the configuration coefficient of 0.662 contributes to the absorption at 415 nm. Table 2 shows that MO 89a′ has 44.6% d_{xy}(Ir), 43.0% π(Mebib), 5.9% π(ppy), and 6.5% π(Cl), while MO 53a″ is a π*(Mebib) type orbital. Thus the absorption at 415 nm is mainly attributed to a {[d_{xy}(Ir) + π(Mebib)] → [π*(Mebib)]} transition with MLCT/ILCT transition character, while the absorption at 399 nm of **3** has a similar transition character to that of **1** at 415 nm. For **2**, the absorption at 439 nm has a different transition character from that of **1** and **3**. Table 5 shows that the excitation of MO 92a′ → MO 53a″ (CI = 0.685) is the dominant contribution to the absorption band at 439 nm. Table 3 shows that MO 92a′ is composed of 42.4% d_{xy}(Ir), 33.2% π(Mebib), 9.1% π(ppy), and 15.3% π(C≡CH), thus this absorption transition can be described as a {[d_{xy}(Ir) + π(Mebib) + π(C≡CH)] → [π*(Mebib)]} transition with MLCT/ILCT/XLCT transition character.

Table 5 also shows that the excitation of MO 88a′ → MO 53a″ contributes to the $X\,^1A' \rightarrow C\,^1A'$ absorption of **1** at 321 nm. Table 2 shows that MO 88a′ is mainly composed of 69.3% π(Mebib) and 15.8% π(Cl), so this transition can be described as a {[π(Mebib) + π(Cl)] → [π*(Mebib)]} transition with ILCT/XLCT transition character. The absorption band of **2** at 332 nm has a transition path similar to that of **1** at 321 nm. But that of **3** at 316 nm is assigned to a {[π(Mebib) + π(ppy)] → [π*(Mebib)]} transition with different ILCT/LLCT transition character (see Table 4). The absorptions at 260 and 262 nm for **1** and **2** are from several excitations which are attributed to {[d_{yz}(Ir) + π(Mebib) + π(ppy) + π(X)] → [π*(ppy)]} combined transitions, but that of **3** at 252 nm has a transition character similar to its first two lowest lying absorptions. The calculated vertical triplet lowest lying absorptions of **1**, **2**, and **3** at 526 nm (2.36 eV), 532 nm (2.33 eV), and 504 nm (2.46 eV), respectively, are all assigned to a ^{3}[d_{yz}(Ir) + π(Mebib) + π(X)] → ^{3}[π*(Mebib)]} transition with ^{3}MLCT/^{3}LLCT/^{3}XLCT character (see Table 5).

The UV-vis spectrum of **1** in CH_2Cl_2[15] shows the ^{1}MLCT band at 472 nm in addition to the ππ* transition at 244 nm for the ppy ligand, and transitions at 299 and 360 nm for the Mebib ligand, which are consistent with our calculated absorption bands at 444, 260 nm, and 321 nm. The calculated ^{3}MLCT absorption bands of **1** and **3** at 526 and 504 nm attributed to ^{3}MLCT/^{3}LLCT/^{3}XLCT transitions are consistent with the measured triplet absorption bands at 523 and 506 nm assigned to ^{3}MLCT.

Geometries in the triplet excited state and emission in CH_2Cl_2 media

The main geometry structural parameters of **1–3** in the $A\,^3A'$ excited state are given in Table 1. The calculated results show that the bond lengths, bond angles, and dihedral angles in the excited state are slightly changed relative to those in the ground state, however, the three complexes show a similar variation trend. The calculated Ir–N(1), Ir–C(1), Ir–N(3), Ir–C(2), and Ir–X bond lengths relax by about 0.02–0.03 Å, which indicates that the ppy, Mebib, and X ligands tend to break away from the Ir atom in the excited state. The calculated bond angles change by about 1° compared with those in the ground state. The C(1)–C(3)–C(4)–N(2) dihedral angle is still close to 0°, which indicates that the Mebib ligand keeps its planar structure in the excited state. The slight changes in the geometry result from electron excitation from the ppy–Ir–X bonding orbital to the π*(Mebib) orbital (*vide infra*) upon excitation.

The stretching frequencies of ν(Ir–Cl), ν(Ir–C(1)), ν(Ir–C(2)), ν(Ir–C(5)), ν(Ir–N(1)), and ν(Ir–N(3)) for **1–3** in the ground and excited state are calculated at the same theory level. With respect to **3**, the stretching frequency of ν(Ir–N(l)) at 954 cm^{-1} in the ground state decreases to 951 cm^{-1} in the excited state, which indicates that there is a weaker bonding interaction between Ir and N(1) in the excited state than that in the ground state, and is consistent with the relaxation *ca.* 0.026 Å in the bond length of Ir–N(1). Variation in the other stretching frequency is similar to that seen for ν(Ir–N(1)), and complexes **1** and **2** display similar variations to those seen for **3**.

 This journal is © The Royal Society of Chemistry 2007

View Article Online

Published on 23 March 2007. Downloaded by Michigan State University on 21/01/2016 12:05:07.

Table 6 The calculated phosphorescent emissions of **1–3** determined using the TDDFT method, together with the corresponding experimental values

	Emission	Transition	Config. (CI coeff)	E/nm (eV)	E_{exptl}/nm (eV)[a]
1	$A^3A' \rightarrow X^1A'$	53a″ → 52a″ (0.675)	565 (2.19)	555 (2.23)
2	$A^3A' \rightarrow X^1A'$	53a″ → 52a″ (0.678)	576 (2.15)	
3	$A^3A' \rightarrow X^1A'$	53a″ → 52a″ (0.660)	543 (2.28)	526 (2.36)

[a] From ref. 15.

Table 7 Molecular orbital compositions (%) in the A^3A excited states for **1–3** at the B3LYP level of theory

		MO composition				
Orbital	Energy/eV	Ir	Mebib	ppy	X	Main bond nature
1						
53a″	−1.9364	1.6	98.0	0.4	0.0	π*(Mebib)
52a″	−5.1925	50.7	26.8	17.0	5.5	d_{yz}(Ir) + π*(Mebib) + π*(ppy)
2						
53a″	−1.8888	1.6	98.0	0.3	0.1	π*(Mebib)
52a″	−5.0622	51.3	24.7	13.5	10.5	d_{yz}(Ir) + π*(Mebib) + π*(ppy) + π*(C≡CH)
3						
53a″	−1.9745	1.4	98.3	0.2	0.1	π*(Mebib)
52a″	−5.401	47.3	32.3	17.6	2.8	d_{yz}(Ir) + π*(Mebib) + π*(ppy)

The calculated phosphorescence emissions of **1–3** in CH_2Cl_2 media together with the measured values[15] are given in Table 6; the frontier molecular orbital compositions responsible for the emissions are compiled in Table 7.

The calculated phosphorescence values of 565 nm (2.19 eV), 576 nm (2.15 eV), and 543 nm (2.28 eV), for **1–3**, respectively, agree well with their respective experimental values[15] of 555 nm (2.23 eV) and 526 nm (2.36 eV) for **1** and **3**. With respect to **1**, the excitation of MO 53a″ → MO 52a″ with the configuration coefficient of 0.675 causes the emission at 565 nm. Table 7 shows that MO 53a″ has a contribution of 98.0% π*(Mebib), while MO 52a″ is composed of 50.7% d_{yz}(Ir), 26.8% π(Mebib), 17.0% π(ppy), and 5.5% π(Cl). Another excitation of MO 53a″ → MO 50a″ (CI = 0.317) has some other contributions, MO 50a″ has 72.5% π(Mebib) and 23.0% π(ppy). Thus the emission of **1** at 565 nm originates from the ^{3}\{[d_{yz}(Ir) + π(Mebib) + π(ppy) + π(Cl)] [π*(Mebib)]\} excited state with ^{3}MLCT/^{3}ILCT/^{3}LLCT and little ^{3}XLCT character. The emission of **3** at 543 nm has a transition character similar to that of **1** at 565 nm. For the emission of **2** at 576 nm, Table 7 shows that the contribution to the MO 52a″ orbital by the π(C≡CH) orbital is 10.5% which is higher than in other complexes, therefore indicating that the ^{3}XLCT transition is of more importance and larger in **2** than other complexes. To intuitively understand the emission transition, we display the electron density diagrams of **1** in Fig. 4. Comparing **1** with **2** and **3**, the ^{3}XLCT transition composition increases in the order **3** < **1** < **2** along with the reverse order of the increasing π electron-withdrawing ability of X ligands –C≡CH<–Cl<–CN. The emission results indicate that ligand X can participate in the emission transition and the ^{3}XLCT transition will occupy larger composition when the π electron-withdrawing ability of ligand X is decreased, which results in the red shift of the emission spectra of **1** and **2** compared with that of **3**. There is no experimental assignment for the emission so the calculations extend the experimental results.

The discussion of the absorption reveals that the lowest lying absorptions calculated for **1** and **3** at 444 and 416 nm, respectively, arise mainly from MLCT/ILCT/LLCT transitions and the absorption of **2** at 458 nm is assigned to MLCT/ILCT/LLCT with a larger XLCT transition than those of **1** and **3**, while the calculated phosphorescence values are just the reverse processes of these lowest lying absorptions due to the same transition character and symmetry. The energy differences between the calculated lowest lying absorptions and corresponding phosphorescences are 0.57, 0.56, and 0.7 eV for **1–3**, respectively, which is consistent with the measured Stokes shifts of 0.40 and 0.64 eV for **1** and **3**.[15]

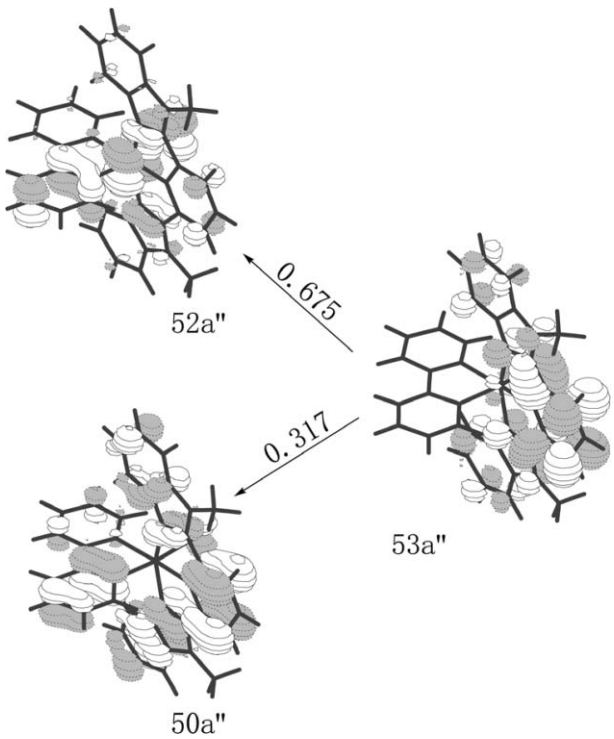

Fig. 4 Single electron transition with |CI coefficients | > 0.1 from TDDFT/LANL2DZ calculations for the 565 nm emission of complex **1** in CH_2Cl_2.

View Article Online

Published on 23 March 2007. Downloaded by Michigan State University on 21/01/2016 12:05:07.

Obviously, both the calculated and experimental results show that the phosphorescence can be tuned by changing the π electron-withdrawing ability of ligand X.[15] Weaker π electron-withdrawing ability will lead to a greater red shift of the absorption and emission spectra.

Conclusions

The present work has investigated the ground and excited state geometries, absorption and phosphorescence properties of three iridium(III) complexes with Mebib, ppy and X (−Cl, –C≡CH, and –CN) ligands theoretically. HOMO of the complexes can be significantly changed by altering the X ligands, but the LUMO is hardly influenced. The lowest lying absorptions of **1** and **3** at 444 and 416 nm are assigned to MLCT/LLCT/ILCT transitions, while the lowest lying absorption of **2** at 458 nm can be described as a MLCT/ILCT/LLCT/XLCT transition. The phosphorescences of **1** and **3** at 565 nm and 543 nm originate from a ^{3}MLCT/^{3}LLCT/^{3}ILCT excited state, while that of **2** at 576 nm is from a ^{3}MLCT/^{3}ILCT/^{3}LLCT/^{3}XLCT excited state. The emission color can be affected by changing π electron-withdrawing ability of the X ligands. So it is very practical to explore the relationship between the X ligand and the phosphorescence of the Ir(III) complexes. We hope these theoretical studies will assist in the design of highly efficient phosphorescent materials.

Acknowledgements

This work was supported by the Natural Science Foundation of China (Grant Nos. 20173021, 20333050, and 20573042).

References

1 (*a*) Y. Wand, N. Herron, V. V. Grushin, D. D. LeCloux and V. A. Petrov, *Appl. Phys. Lett.*, 2001, **79**, 449; (*b*) H. Xin, F. Y. Li, M. Shi, Z. Q. Bian and H. Ch. Huang, *J. Am. Chem. Soc.*, 2003, **125**, 7166; (*c*) A. Tsuboyama, H. Iwawaki, M. Furugori, T. Mukaide, J. Kamatani, S. Igawa, T. Moriyama, S. Miura, T. Takiguchi, S. Okada, M. Hoshino and K. Ueno, *J. Am. Chem. Soc.*, 2003, **125**, 12971.
2 (*a*) K. K. W. Lo, C. K. Chung, T. K. M. Lee, L. H. Lui, K. H. K. Tsang and N. Y. Zhu, *Inorg. Chem.*, 2003, **42**, 6886; (*b*) K. K. W. Lo, D. C. M. Ng and C. K. Chung, *Organometallics*, 2001, **20**, 4999.
3 P. I. Djurovich and M. E. Thompson, *J. Am. Chem. Soc.*, 2001, **124**, 14828.
4 (*a*) N. D. Silaware, A. S. Goldman, R. Ritter and D. R. Tyler, *Inorg. Chem.*, 1989, **28**, 1231; (*b*) K. A. Belmore, R. A. Vanderpool, J. C. Tsai, M. A. Khan and K. M. Nicholas, *J. Am. Chem. Soc.*, 1988, **110**, 2004.
5 C. Adachi, M. A. Baldo, S. R. Forrest and M. E. Thompson, *Appl. Phys. Lett.*, 2000, **77**, 904.
6 S. Lamansky, P. Djurovich, D. Murphy, F. Abdel–Razzaq, H. E. Lee, C. Adachi, P.E. Burrows, S. R. Forrest and M. E. Thompson, *J. Am. Chem. Soc.*, 2001, **123**, 4304.
7 S. Lamansky, P. Djurovich, D. Murphy, F. Abdel-Razzaq, R. Kwong, I. Tsyba, M. Bortz, B. Mui, R. Bau and M. E. Thompson, *Inorg. Chem.*, 2001, **40**, 1704.
8 P. J. Hay, *J. Phys. Chem. A*, 2002, **106**, 1634.
9 (*a*) J. P. J. Markham, S. C. Lo, S. W. Magennis, P. L. Burn and I. D. W. Samuel, *Appl. Phys. Lett.*, 2002, **80**, 2645; (*b*) C. Adachi, M. A. Baldo and S. R. Forrest, *Appl. Phys. Lett.*, 2000, **77**, 904; (*c*) M. G. Colombo and H. U. Gudel, *Inorg. Chem.*, 1993, **32**, 3081; (*d*) M. A. Baldo, S. Lamansky, P. E. Burrows, M. E. Thompson and S. R. Forrest, *Appl. Phys. Lett.*, 1999, **75**, 4.
10 J. C. Ostrowski, M. R. Robinson, A. J. Heeger and G. C. Bazan, *Chem. Commun.*, 2002, 784.
11 K. A. King, P. J. Spellane and R. J. Watts, *J. Am. Chem. Soc.*, 1985, **107**, 1431.
12 A. B. Tamayo, B. D. Alleyne, P. I. Djurovich, S. Lamansky, I. Tsyba, N. N. Ho, R. Bau and M. E. Thompson, *J. Am. Chem. Soc.*, 2003, **125**, 7377.
13 (*a*) J. P. Collin, I. M. Dixon, J. P. Sauvage, J. A. G. Williams, F. Barigelletti and L. Flamigni, *J. Am. Chem. Soc.*, 1999, **121**, 5009; (*b*) I. M. Dixon, J. P. Collin, J. P. Sauvage and L. Flamigni, *Inorg. Chem.*, 2001, **40**, 5507.
14 Md. K. Nazeeruddin, R. Humphry–Baker, D. Berner, S. Rivier, L. Zuppiroli and M. Graetzel, *J. Am. Chem. Soc.*, 2003, **125**, 8790.
15 S. Obara, M. Itabashi, F. Okuda, S. Tamaki, Y. Tanabe, Y. Ishii, K. Nozaki and M. A. Haga, *Inorg. Chem.*, 2006, **45**, 8907.
16 (*a*) R. E. Stratmann and G. E. Scuseria, *J. Chem. Phys.*, 1998, **109**, 8218; (*b*) N. N. Matsuzawa and A. Ishitani, *J. Phys. Chem. A*, 2001, **105**, 4953; (*c*) M. E. Casida, C. Jamorski, K. C. Casida and D. R. Salahub, *J. Chem. Phys.*, 1998, **108**, 4439.
17 E. Runge and E. K. U. Gross, *Phys. Rev. Lett.*, 1984, **52**, 997.
18 A. D. Becke, *J. Chem. Phys.*, 1993, **98**, 5648.
19 (*a*) J. F. Stanton, J. Gauss, N. Ishikawa and M. Head-Gordon, *J. Chem. Phys.*, 1995, **103**, 4160; (*b*) J. B. Foreman, M. Head-Gordon and A. Pople, *J. Phys. Chem.*, 1992, **96**, 135; (*c*) V. A. Waiters, C. M. Hadad, Y. Thiel, S. D. Colson, K. B. Wibergy, P. M. Johnson and J. B. Foresman, *J. Am. Chem. Soc.*, 1991, **113**, 4782.
20 (*a*) M. Cossi, G. Scalmani, N. Regar and V. Barone, *J. Chem. Phys.*, 2002, **117**, 43; (*b*) V. Barone and M. Cossi, *J. Chem. Phys.*, 1997, **107**, 3210.
21 (*a*) T. Liu, B. H. Xia, X. Zhou, H. X. Zhang, Q. J. Pan and J. S. Gao, *Organometallics*, 2007, **26**, 143; (*b*) X. Zhou, H. X. Zhang, Q. J. Pan, B. H. Xia and A. C. Tang, *J. Phys. Chem. A*, 2005, **109**, 8809; (*c*) L. Yang, J. K. Feng and A. M. Ren, *Synth. Met.*, 2005, **152**, 265.
22 (*a*) P. J. Hay and W. R. Wadt, *J. Chem. Phys.*, 1985, **82**, 299; (*b*) P. J. Hay and W. R. Wadt, *J. Chem. Phys.*, 1985, **82**, 270.
23 M. J. Frisch, G. W. Trucks, H. B. Schlegel, G. E. Scuseria, M. A. Robb, J. R. Cheeseman, J. A. Montgomery, Jr., T. Vreven, K. N. Kudin, J. C. Burant, J. M. Millam, S. S. Iyengar, J. Tomasi, V. Barone, B. Mennucci, M. Cossi, G. Scalmani, N. Rega, G. A. Petersson, H. Nakatsuji, M. Hada, M. Ehara, K. Toyota, R. Fukuda, J. Hasegawa, M. Ishida, T. Nakajima, Y. Honda, O. Kitao, H. Nakai, M. Klene, X. Li, J. E. Knox, H. P. Hratchian, J. B. Cross, C. Adamo, J. Jaramillo, R. Gomperts, R. E. Stratmann, O. Yazyev, A. J. Austin, R. Cammi, C. Pomelli, J. W. Ochterski, P. Y. Ayala, K. Morokuma, G. A. Voth, P. Salvador, J. J. Dannenberg, V. G. Zakrzewski, S. Dapprich, A. D. Daniels, M. C. Strain, O. Farkas, D. K. Malick, A. D. Rabuck, K. Raghavachari, J. B. Foresman, J. V. Ortiz, Q. Cui, A. G. Baboul, S. Clifford, J. Cioslowski, B. B. Stefanov, G. Liu, A. Liashenko, P. Piskorz, I. Komaromi, R. L. Martin, D. J. Fox, T. Keith, M. A. Al-Laham, C. Y. Peng, A. Nanayakkara, M. Challacombe, P. M. W. Gill, B. W. Johnson Chen, M. W. Wong, C. Gonzalez and J. A. Pople, *Gaussian 03, Revision C.02*, Gaussian, Inc., Wallingford, CT, 2004.

 This journal is © The Royal Society of Chemistry 2007